RESEARCH ARTICLE

Effect of component activity of plant cells on plant growth rate

Mingjuan Bi[1, *], Yingying Cui[1], Qinyong Su[1], Zhenxue Tang[1], Jingcong Tao[1], Fushan Zheng[2]

[1]Department of Pharmaceutical and Food Science, [2]Scientific Research Office, Laiwu Vocational and Technical College, Jinan, Shandong, China.

Received: August 8, 2025; **accepted:** November 25, 2025.

The physiological activity of plant cells is a key internal factor influencing their growth and development. However, the mechanism by which the specific activities of different intracellular components synergistically regulate the overall growth rate of plants remains unclear. To clarify this issue, this study aimed to systematically explore the influence of the activity of core components of plant cells on the growth rate of plants. This study used *Arabidopsis* Col-0 ecological type as the material and set up four groups including control check (CK), low activation group (LA), medium activation group (MA), and high activation group (HA). The activities of antioxidant enzymes, metabolic enzymes, metabolite content, as well as growth indicators such as plant height, leaf area, biomass, and net photosynthetic rate in cellular components were measured, and correlation analysis was conducted. The results demonstrated that the plant height of the HA reached 18.4 ± 1.6 cm on the 28th day, significantly higher than the 12.3 ± 1.5 cm of the CK and the 7.6 ± 0.8 cm of the LA. The leaf area of the HA was 55.7 ± 4.5 cm^2, and the net photosynthetic rate was 28.9 μmol/m^2·s, which was 41% outperformed compared to CK. The HA had a dry weight of 0.158 ± 0.015 g in the above-ground part and 0.042 ± 0.005 g in the underground part, both superior to the other groups. In terms of enzyme activity, the superoxide dismutase (SOD) activity in the HA was 300 ± 25 U/mg protein, which was 2.5 times higher than that of the LA. The metabolite glucose content in the HA was 6.5 ± 0.5 μmol/mg protein, which was 3.25 times higher than that in the LA. Correlation analysis showed that growth rate was significantly positively correlated with enzyme activities such as SOD and ATP synthase, as well as metabolite content such as glucose (P < 0.01). This study revealed that the activity of plant cell components enhanced the antioxidant system, improved energy and carbon metabolism activity, promoted photosynthetic efficiency and biomass accumulation, and significantly increased growth rate.

Keywords: plant cells; component activation degree; growth rate; antioxidant enzyme; chlorophyll.

[*]**Corresponding author:** Mingjuan Bi, Department of Pharmaceutical and Food Science, Laiwu Vocational and Technical College, Jinan, Shandong 271100, China. Email: bmjsqy@126.com.

Introduction

Plants are one of the most important life forms on Earth. Studying the regulatory mechanisms of plant growth and development has always been a core issue in life sciences [1]. With the advancement of agricultural modernization and the increasing demand for global food security, exploring how to efficiently promote plant growth has become a key issue that urgently needs to be broken through [2]. Currently, researchers have made progress in analyzing the molecular mechanisms of plant growth from multiple levels including gene expression regulation, hormone signaling, and environmental factor response to improve crop

varieties through genetic modification technology and precisely regulate the plant growth process using plant hormones [3]. However, existing research has mostly focused on macro level regulatory networks, and there is still a lack of systematic exploration of the quantitative relationship between the component activation degree (CAD) and growth rate (GR) in plant cells [4]. The activation status of various biomolecules, metabolites, and organelles within plant cells, which serve as the material basis for cellular life activities, has not yet formed a clear theoretical framework on how their dynamic changes affect the overall GR of plants. In addition, traditional research methods often rely on the measurement of a single indicator, which makes it difficult to fully reflect the multidimensional characteristics and synergistic effects of cellular CAD [5].

Molina *et al*. analyzed the recognition mechanism of polysaccharides released from plant cell wall damage as damage related molecular patterns through molecular biology and biochemistry methods and found that plants perceived cell wall polysaccharides through pattern recognition receptors and activate patterns to trigger immunity [6]. Chieb and Gachomo systematically reviewed the interaction mechanisms between plants and rhizosphere growth-promoting bacteria under drought stress, integrating research data from physiological, biochemical, and molecular levels and found that plants and rhizosphere growth-promoting bacteria enhanced plant drought resistance by promoting root development, regulating plant hormone and antioxidant enzyme activities [7]. Talaat *et al*. applied a new plant growth promoter to barley leaves under salt stress and measured antioxidant enzyme activity (EA), photosynthetic parameters, and membrane damage indicators. The results showed that the new plant growth promoter increased the superoxide dismutase (SOD) activity by 35 - 50% and the chlorophyll content (CpC) by 20 - 30% [8]. Zhao *et al*. utilized abscisic acid signal mutants and exogenous abscisic acid treatment combined with reactive oxygen species detection and programmed cell death analysis to study the physiological changes of rice anthers under high temperature stress. The study found that high temperature induced the accumulation of abscisic acid, triggering an outbreak of reactive oxygen species, leading to premature programmed cell death and pollen abortion in the tapetum layer [9]. Roychowdhury *et al*. reviewed the interaction network between the jasmonic acid (JA) signaling pathway and hormones including salicylic acid (SA) and ethylene and analyzed the regulatory mechanism of JA in plant immunity. The results showed that JA activated defense genes and inhibited pathogenic effectors. Exogenous JA treatment could reduce disease incidence by 30 - 50% [10]. Chu *et al*. identified the gene families of trehalose synthase and phosphatase in peanuts through genome analysis and phylogenetic tree construction. Seventeen trehalose synthase genes and 15 phosphatase genes were found in peanuts, which enhanced cell osmotic regulation ability by accumulating trehalose [11]. Truong *et al*. conducted pot experiments in central Vietnam to compare the effects of silicon fertilizer and biochar (rice husks, peanut shells) on dry matter accumulation and silicon absorption in rice. The results showed that the application of 15 g/kg rice husk biochar increased the aboveground dry matter of rice by 66.7% and the silicon absorption by 40 - 50% [12]. Kumar *et al*. conducted field experiments in the red soil region of West Bengal to evaluate the impact of potato and legume (sesame, barley, *etc*.) rotation on yield and economic benefits. The research revealed that potato barley rotation increased tuber yield by 25% and net income by 30%, while legume crops promoted potato growth through nitrogen fixation and improved soil structure [13].

Current research has revealed some mechanisms of plant growth regulation from macro levels such as gene expression regulation, hormone signaling, and environmental factor response. However, existing research has significant limitations, focusing mainly on macroeconomic regulatory networks, and lacking a systematic exploration of the quantitative relationship

between intracellular biomolecules, metabolites, and organelle activity and GR. In addition, traditional methods rely on a single indicator for measurement, which makes it difficult to fully reflect the multidimensional characteristics and synergistic effects of cellular CAD [14, 15]. This research investigated the CAD impact on GR in plant cells by analyzing the correlation between intracellular CAD dynamics and GR to quantitative analysis of the synergistic effects of biological macromolecules, metabolites, and organelle activation states from multiple dimensions. The results of this study would fill the gap in micro-mechanism research and provide a theoretical basis for the precise regulation of plant growth.

Materials and methods

Seed sterilization and sowing

Arabidopsis Col-0 ecological type obtained from the Genetic Resources Center of the Institute of Botany, Chinese Academy of Sciences, Beijing, China with complete genome sequencing and a short growth cycle about 6 weeks from sowing to maturity was selected as the model plant. All seeds underwent 48 hours of low temperature vernalization treatment at 4℃ before breaking dormancy and promoting germination [16].

Seedling cultivation and treatment

This study adopted a completely randomized experimental design with 4 treatment groups including control check (CK) group, low activity (LA) group, medium activation (MA) group, high activation (HA) group.

(1) CK group

The plant cells were cultured in normal Murashige and Skoog (MS) medium containing 30 g/L sucrose, 8 g/L agar, 0.1 mg/L 6-benzylaminopurine as plant growth regulator, 0.5 mg/L indoleacetic acid, without any CAD regulation treatment.

(2) LA group

RNA interference technology was applied to inhibit the expression of key activating enzyme genes including ATP synthase β subunit (*atpB*) gene and nicotinamide adenine dinucleotide phosphate (NADPH) dehydrogenase gene (*ndhB*) to construct transgenic plants using *Agrobacterium tumefaciens* strain GV3101 (Laboratory of Plant Biotechnology, Institute of Microbiology, Chinese Academy of Sciences, Beijing, China) transformation method. Polymerase chain reaction (PCR) and qRT-PCR were employed to identify the strains with downregulated expression levels of the target gene to around 50% of the wild-type. Both PCR and qRT-PCR were performed using Bio-Rad CFX96 thermal cycler (Bio-Rad Laboratories, Hercules, CA, USA) with *atpB* forward primer as 5'-ATG GCG ACC ACC GAG AAG-3', reverse primer as 5'-TCA GCT CCA CCA CCT TCT C-3' and *ndhB* forward primer as 5'-ATG GCC GAG CTC AAG GAG-3', reverse primer as 5'-TCA CGT CCA CCA CCT TC-3'. PCR reaction included 1× Ex Taq Buffer, 0.2 mM dNTPs, 0.2 μM each primer, 1 U Ex Taq polymerase, and 50 ng template DNA using TaKaRa Ex Taq Kit (TaKaRa Bio, Shiga, Japan) under the program of 94°C for 5 min followed by 35 cycles of 94°C for 30 s, 55°C for 30 s, 72°C for 1 min, and final extension at 72°C for 10 min. The qRT-PCR was performed using the SYBR Green PCR Kit (Thermo Fisher Scientific, Waltham, MA, USA) with the reaction mixture containing 1× SYBR Green Master Mix, 0.2 μM each primer, and 50 ng cDNA under the program of 50°C for 2 min, 95°C for 10 min followed by 40 cycles of 95°C for 15 s and 60°C for 1 min.

(3) MA group

The plant cells were treated with 50 μM salicylic acid as a chemical inducer to enhance cellular CAD by activating the SA signaling pathway. Starting from the 7th day after sowing, the roots were soaked in 1/2 strength MS liquid medium containing SA for 30 minutes per week.

(4) HA group

ndhB overexpression plasmid (pCAMBIA1301 ndhB) was constructed by combining gene overexpression and chemical treatment using

pCAMBIA1301 vector (Cambia, Canberra, ACT, Australia). 100 µM methyl jasmonate (Sigma-Aldrich, St. Louis, MO, USA) was applied to plant cells from the 7th day after sowing to synergistically improve CAD.

All treatments were conducted for 3 replicates in each group with 50 seedlings being planted in each replicate.

Sample collection

Leaf samples were collected at 0, 7, 14, 21, and 28 days, frozen in liquid nitrogen, and stored at -80°C for CAD measurement. Morphological and physiological indicators were recorded simultaneously.

Cell component separation

About 0.5 g of fresh leaves were cut from *Arabidopsis thaliana* seedlings that were grown for 14 days. The samples were washed 3 times with pre-cooled PBS buffer to remove surface impurities. After absorbing the water, it was placed in a pre-cooled mortar and quickly ground into a fine powder by adding liquid nitrogen [17]. Subcellular components were extracted by transferring ground powder to a 5 mL centrifuge tube before adding 2 mL of extraction buffer containing protease inhibitor (100 mM Tris HCl, pH 8.0, 50 mM $MgCl_2$, 1 mM EDTA). The mixture was gently vortexed and mixed for 30 min in an ice bath followed by centrifuging at 10,000 g for 15 min at 4℃ using Eppendorf 5415R centrifuge (Eppendorf, Hamburg, Germany). The supernatant was collected as cytoplasmic component. After precipitation, the pellet was washed twice with extraction buffer followed by adding 1 mL of buffer containing 0.1% Triton X-100 and sonicating in an ice bath with 300 W, pulse 3s/interval 3 s, for 10 times using Sonics VCX 500 ultrasonic cell disruptor (Sonics & Materials, Inc., Newtown, CT, USA). The reaction was then centrifuged at 15,000 g for 20 minutes at 4℃. The supernatant consisted of organelle components including mitochondria, chloroplasts, *etc*. was collected. The bicinchoninic acid (BCA) protein assay kit (Thermo Fisher Scientific, Waltham, MA, USA) was used to determine the protein concentrations of each component utilizing bovine serum albumin (BSA) as the standard to ensure consistent sample concentrations for subsequent activity assays [18].

Key enzyme activation detection

(1) SOD

SOD was determined by nitroblue tetrazolium (NBT) photochemical reduction method. The reaction system consisted of 50 mM phosphate buffer (PB) (pH 7.8), 13 mM methionine, 75 µM NBT, 20 µM riboflavin, and 10 µL enzyme solution with a total volume of 3 mL. After mixing, the solution was reacted for 20 minutes under 4,000 lux light. After terminating the reaction in the dark, the absorbance at 560 nm was measured to determine the EA unit (U) that inhibited 50% of NBT photochemical reduction [19].

(2) Peroxidase (POD)

POD was determined using the guaiacol method. The reaction included 50 mM PB (pH 6.0), 20 mM guaiacol, 10 mM H_2O_2, and 10 µL enzyme solution with overall volume of 3 mL. After incubating at 25℃ for 5 minutes, the changes of absorbance at 470 nm were measured with a increase of 0.01 absorbance/min as one EA unit [20].

(3) Adenosine triphosphate (ATP) synthase

ATP synthase was determined by mixing 20 µL of organelle components with 100 µL of detection buffer before adding 50 µL of fluorescein luciferase reagent. The fluorescence intensity was measured immediately by using Hitachi F-7000 fluorescence spectrophotometer (Hitachi High Technologies, Tokyo, Japan) with excitation wavelength of 560 nm and emission wavelength of 590 nm. The ATP concentration generated by the enzymatic reaction was calculated based on the ATP standard curve. The EA was expressed as the ATP (nmol/mg·min).

(4) NADPH dehydrogenase

The reaction contained 100 mM Tris-HCl (pH 7.5), 1 mM $NADP^+$, 1 mM glucose-6-phosphate, 10 µL of cytoplasmic components for a total of 1 mL. After incubating for 10 min at 25°C, the NADPH

generation rate was measured at 340 nm with an absorbance change of 0.01 per min as one EA unit [21].

Metabolite activity assessment

High-performance liquid chromatography (HPLC) analysis was performed using an Agilent 1260 Infinity system (Agilent Technologies, Santa Clara, CA, USA) to analyze the concentration of major metabolites in cells under the conditions of C18 column (250 × 4.6 mm, 5 μm), mobile phase of 50 mM potassium dihydrogen phosphate (pH 2.5):methanol (95:5, v/v), flow rate of 1.0 mL/min, column temperature of 30℃, injection volume of 10 μL, UV detector wavelength of 210 nm. Measurement indicators included glucose, fructose, pyruvic acid, malic acid, citric acid, *etc*. The activation level was expressed as the content of each metabolite in the unit protein (μmol/mg).

Morphological index determination

Plant height (PH) was measured as the vertical distance from the seedling base (cotyledon attachment) to the top growth point once a week for 4 weeks using a Mitutoyo 500-196-30 vernier caliper (Mitutoyo Corporation, Kawasaki, Japan) with a precision of 0.1 mm. 30 plants from each treatment group were measured, and the average value was taken. The leaf area (L-A) was measured by using LI-3000C L-A analyzer to scan and measure the fully unfolded leaves of the plant. The total L-A of each plant was recorded weekly. The young leaves were estimated using the product of length and width method. The biomass was measured by collecting the entire seedling at 7, 14, 21, and 28 days after sowing. After washing with deionized water, the samples were divided into aboveground and underground parts. After incubating at 105℃ for 30 min, the samples were dried at 70℃ to constant weight. The dry weight (DW) was measured using Sartorius CPA225D analytical balance (Sartorius AG, Göttingen, Germany) with the accuracy of 0.1 mg.

Monitoring of physiological indicators

The photosynthetic rate was measured using LI-6400 portable photosynthesis analyzer (LI-COR Biosciences, Lincoln, NE, USA). Fully unfolded leaves were selected to measure the net photosynthetic rate (Pn) from 9:00 to 11:00 in the morning with the light intensity of 1,000 μmol/m^2·s, CO_2 concentration of 400 μmol/mol, temperature of 22 ± 1℃, and humidity of 60 ± 5%. 10 leaves from each treatment were measured, and the average values were calculated. CpC was determined by the ethanol extraction method. Briefly, 0.1 g of leaves were cut into pieces before 10 mL of 95% ethanol being added and extracted for 24 h in the dark until the leaves totally turning white. The absorbances at 665 nm and 649 nm were obtained, and the chlorophyll-a, chlorophyll-b, and total CpC were calculated according to the Arnon formula.

GR calculation

The absolute GR (AGR) and relative GR (RGR) were calculated as follows.

$$\begin{cases} AGR = (W_2 - W_1)/(t_2 - t_1) \\ RGR = (ln\, W_2 - ln\, W_1)/(t_2 - t_1) \end{cases} \quad (1)$$

where W_1 and W_2 were the biomass (DW) at time t_1 and t_2 and were measured in g/d.

Data analysis

SPSS 26.0 (IBM, Armonk, New York, USA) was employed for statistical analysis with data expressed as mean ± standard deviation. The comparison of inter-group differences was conducted using one-way analysis of variance (ANOVA). If the variance analysis was significant with the *P* value less than 0.05, Duncan's new complex extreme difference method was further utilized for multiple comparisons.

Results and discussion

Comparison of plant GR

The results demonstrated that the GR of *Arabidopsis* varied significantly among treatment groups. The dynamic plant height (PH) changes for each group showed that the PH of CK remained stable as 12.3 ± 1.5 cm by day 28. LA

Table 1. Leaf area (L-A) and the net photosynthetic rate (Pn) of different treatment groups.

Index	Treatment	Day			
		7	14	21	28
L-A (cm^2)	CK	4.3 ± 0.6	12.8 ± 1.5	23.5 ± 2.5	35.6 ± 3.2
	LA	2.5 ± 0.4	7.2 ± 0.9	13.8 ± 1.6	20.1 ± 2.1
	MA	5.8 ± 0.8	17.6 ± 2.0	31.4 ± 3.0	48.3 ± 4.1
	HA	6.5 ± 0.9	19.7 ± 2.2	36.8 ± 3.3	55.7 ± 4.5
Pn ($\mu mol/m^2 \cdot s$)	CK	18.3 ± 1.5	22.1 ± 1.8	20.5 ± 1.6	12.5 ± 1.2
	LA	10.5 ± 1.1	12.3 ± 1.3	11.0 ± 1.0	8.2 ± 0.9
	MA	22.4 ± 1.8	26.7 ± 2.0	25.3 ± 1.9	15.6 ± 1.4
	HA	25.8 ± 2.1	30.5 ± 2.3	28.9 ± 2.2	18.2 ± 1.6

grew slowly with a PH of only 7.6 ± 0.8 cm on day 28, significantly lower than CK ($P < 0.05$). MA and HA grew rapidly with MA reaching 15.8 ± 1.2 cm and HA reaching 18.4 ± 1.6 cm on the 28th day, significantly higher than CK ($P < 0.05$) (Figure 1).

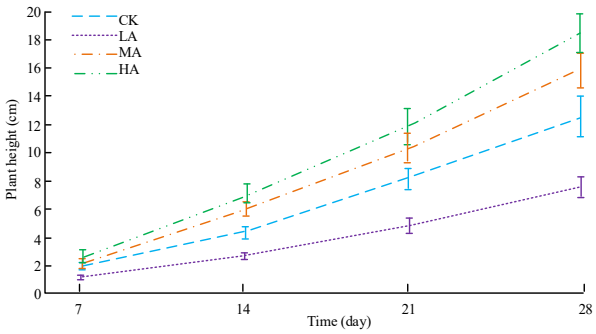

Figure 1. Dynamic changes in PH among different treatment groups.

The leaf area (L-A) and the net photosynthetic rate (Pn) of different treatment groups showed that the trend of L-A changes was similar to that of PH. The total L-A of CK was 35.6 ± 3.2 cm^2 on the 28th day, while the L-A growth of LA was limited, only 20.1 ± 2.1 cm^2. The L-A of MA and HA significantly increased with the MA group reaching 48.3 ± 4.1 cm^2 and HA reaching 55.7 ± 4.5 cm^2. The results indicated that cellular CAD was closely related to L-A expansion. Pn significantly increased with the increase of activity level with HA reaching 28.9 $\mu mol/m^2 \cdot s$ on the 28th day, which was 41% higher than that of CK, indicating that HA level promoted photosynthetic efficiency (Table 1).

The comparison of CpC and metabolite content among different treatment groups demonstrated a positive correlation between CpC and activation degree (AD) (Figure 2a). The total CpC of HA reached 3.80 mg/g, which was 2.3 times that of LA. The chlorophyll a/b ratio was 2.73, higher than that of CK (2.72), which might be related to the optimization of chloroplast thylakoid structure. Pyruvic acid, malic acid, and citric acid are key intermediate products in glycolysis and the tricarboxylic acid cycle, and their contents significantly increase with increasing activity. The pyruvate content of HA was 2.31 µmol/mg, which was three times that of LA, indicating enhanced cellular respiration and carbon metabolism activity (Figure 2b). The dynamic changes in biomass of different treatment groups showed that the dry weights (DW) of the above-ground and the underground parts of CK were 0.085 ± 0.009 g and 0.022 ± 0.003 g on day 28, respectively. The biomass of LA was significantly lower than CK with an aboveground part of 0.041 ± 0.005 g and an underground part of 0.012 ± 0.002 g. The biomass of MA and HA increased significantly with an above-ground part of MA as 0.126 ± 0.012 g and an underground part of 0.035 ± 0.004 g, while the above-ground part of HA was 0.158 ± 0.015 g, and the underground part was 0.042 ± 0.005 g (Figure 3). The AGR and RGR of HA were the highest at 0.0052 ± 0.0005 g/d and 0.045 ± 0.005 g/d, respectively. The AGR and RGR of LA were the lowest at 0.0013 ± 0.0002 g/d and 0.012 ± 0.002 g/d, respectively. CK and MA were in the middle with the AGR and RGR values of 0.0027 ±

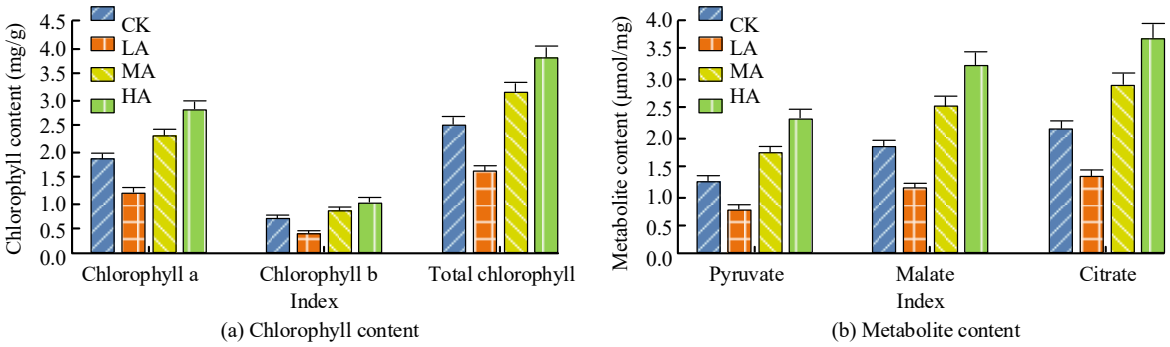

Figure 2. Changes in CpC and metabolite content in various groups.

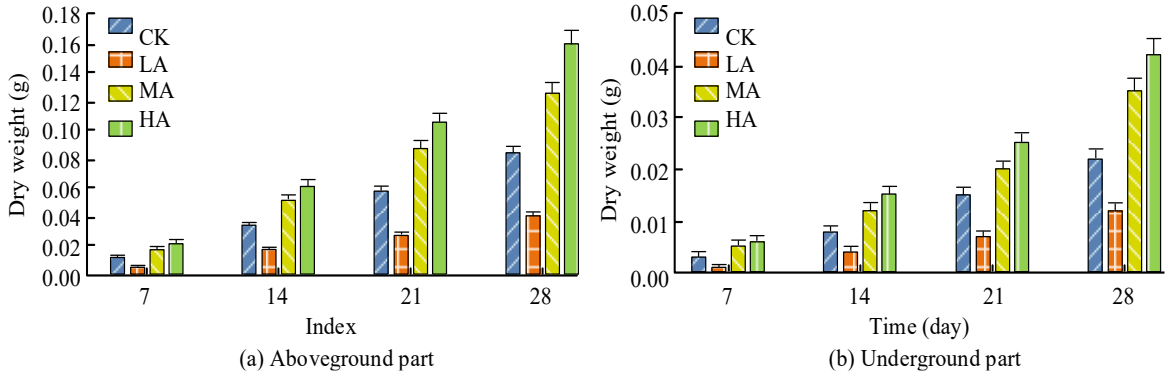

Figure 3. Dynamic changes in biomass of different groups.

0.0003 g/d, 0.025 ± 0.003 g/d, and 0.0040 ± 0.0004 g/d, 0.038 ± 0.004 g/d, respectively. The higher the cellular CAD, the faster the plant GR. There was an obvious active correlation between cellular CAD and plant GR. The PH, L-A, and biomass of the LA were lower than the CK with the PH only 7.6 ± 0.8 cm and the above-ground DW only 0.041 ± 0.005 g on the 28th day. The HA grew the fastest with a PH of 18.4 ± 1.6 cm, above-ground DW of 0.158 ± 0.015 g, and AGR and RGR of 0.0052 g/d and 0.045 g/d, respectively.

Detection of cellular CAD

The AD of the antioxidant enzyme system in four treatment groups demonstrated that LA had the lowest superoxide dismutase (SOD) at 120 ± 10 U/mg protein, while CK had 180 ± 15 U/mg protein. MA and HA showed significant increases in SOD at 250 ± 20 U/mg protein and 300 ± 25 U/mg protein. The ATP synthase activities were 2.5 ± 0.3, 4.0 ± 0.4, 6.0 ± 0.5, and 8.0 ± 0.6 nmol/mg·min for LA, CK, MA, and HA, respectively (Figure 4a). For peroxidase (POD), LA had 80 ± 8 U/mg protein, while CK had 130 ± 12 U/mg protein, and MA had 180 ± 15 U/mg protein, and HA had 220 ± 18 U/mg protein. The NADPH dehydrogenase activities were 15 ± 2, 25 ± 3, 35 ± 4, and 45 ± 5 U/mg protein for LA, CK, MA, and HA., respectively (Figure 4b). The data showed that activation treatment significantly affected the activity of metabolism-related enzymes. The results of metabolite activity evaluation showed that the glucose contents were 2.0 ± 0.2, 3.5 ± 0.3, 5.0 ± 0.4, and 6.5 ± 0.5 μmol/mg protein for LA, CK, MA, and HA, respectively (Figure 5). The content of metabolites such as fructose and pyruvate also showed a similar trend, increasing with the increase of cellular CAD. The increase in enzymatic activity promoted growth by enhancing the activity of antioxidant enzymes

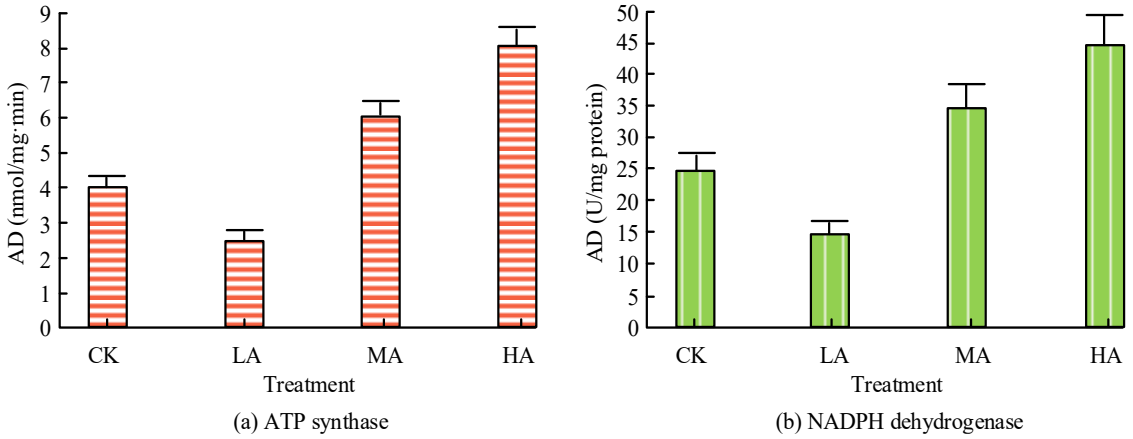

Figure 4. Activation degree (AD) of antioxidant enzyme system in different treatment groups.

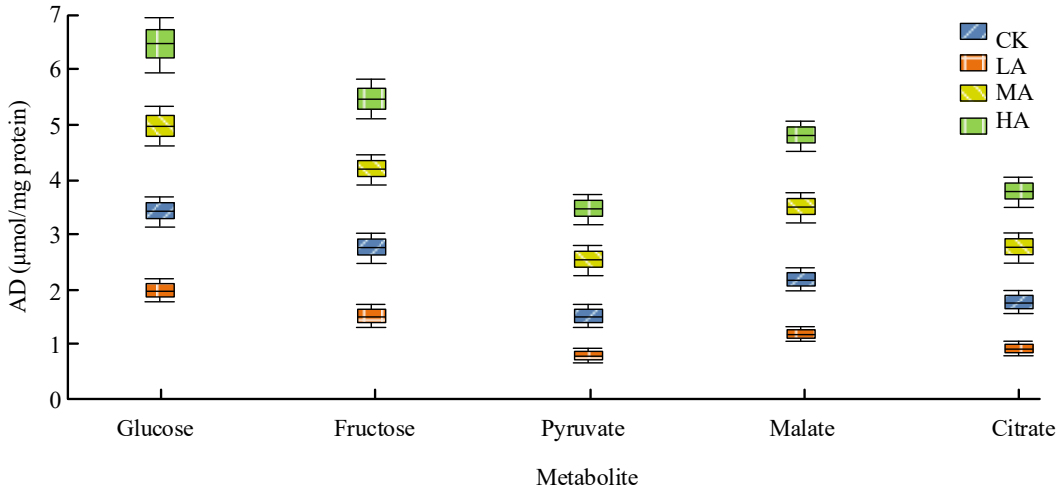

Figure 5. Metabolite activity assessment results.

and metabolic enzymes, optimizing carbon metabolism. The SOD activity of HA reached 300 ± 25 U/mg protein, and the ATP synthase activity was 8.0 ± 0.6 nmol/mg·min, both of which were more than 2.5 times that of LA. The content of metabolites such as glucose and pyruvic acid significantly increased with the increase of enzymatic activity with HA pyruvic acid content reaching 2.31 μmol/mg, which was three times that of LA. Correlation analysis showed that indicators such as PH and biomass were significantly positively correlated with SOD, ATP synthase activity, and metabolite content (P < 0.01) with correlation coefficients (CCs) ranging from 0.82 to 0.90.

Correlation analysis between CAD and GR

The analysis between cellular CAD indicators and plant morphological indicators demonstrated that the PH was positively correlated with SOD EA, ATP synthase activity, glucose content (P < 0.01) with CCs of 0.85, 0.88, and 0.82, respectively. The L-A was significantly positively correlated with POD EA, NADPH dehydrogenase activity, fructose content (P < 0.01) with CCs of 0.83, 0.86, and 0.81, respectively (Table 2). The correlation analysis between biomass and cellular CAD indicators showed that the biomass was significantly positively correlated with the antioxidant enzyme system, metabolic EA, and metabolite content (P < 0.01). The CC between

Table 2. Correlation analysis between cellular CAD indicators and plant morphological indicators.

Parameter	PH		L-A	
	CC	*P*	CC	*P*
SOD activity	0.85	< 0.01	0.78	< 0.05
POD activity	0.78	< 0.05	0.83	< 0.01
ATP synthase activity	0.88	< 0.01	0.76	< 0.05
NADPH dehydrogenase activity	0.80	< 0.01	0.86	< 0.01
Glucose content	0.82	< 0.01	0.72	< 0.05
Fructose content	0.76	< 0.05	0.81	< 0.01

Table 3. Correlation analysis between biomass and cellular CAD indicators.

Parameter	Aboveground DW		Underground DW	
	CC	*P*	CC	*P*
SOD activity	0.86	< 0.01	0.82	< 0.01
POD activity	0.80	< 0.01	0.84	< 0.01
ATP synthase activity	0.89	< 0.01	0.85	< 0.01
NADPH dehydrogenase activity	0.83	< 0.01	0.87	< 0.01
Glucose content	0.84	< 0.01	0.81	< 0.01
Fructose content	0.81	< 0.01	0.79	< 0.01

Table 4. Correlation results between GR and cellular CAD indicators.

Parameter	AGR		RGR	
	CC	*P*	CC	*P*
SOD activity	0.87	< 0.01	0.84	< 0.01
POD activity	0.82	< 0.01	0.85	< 0.01
ATP synthase activity	0.90	< 0.01	0.87	< 0.01
NADPH dehydrogenase activity	0.85	< 0.01	0.88	< 0.01
Glucose content	0.86	< 0.01	0.83	< 0.01
Fructose content	0.83	< 0.01	0.80	< 0.01

above-ground DW and SOD EA was 0.86, and the CC with ATP synthase activity was 0.89. The CC between underground DW and POD EA was 0.84, and the CC with NADPH dehydrogenase activity was 0.87 (Table 3). The correlation analysis between GR and cellular CAD indicators revealed that AGR and RGR were significantly positively correlated with cellular CAD indicators ($P < 0.01$). The CC between AGR and SOD EA was 0.87, and the CC with ATP synthase activity was 0.90. The CC between RGR and POD EA was 0.85, and the CC with NADPH dehydrogenase activity was 0.88 (Table 4).

Functional verification of key components

To further validate the functions of key components, in-depth analysis was conducted on transgenic plants and chemically treated plants. The changes in key gene expression levels and hormone content demonstrated that an obvious increase in the expression level of NADPH dehydrogenase gene (*ndhB*) was observed in the HA with the relative expression degree of 5.6 ± 0.5 compared to 1.0 ± 0.1 in the CK (Figure 6a). The expression level of *atpB* gene was significantly downregulated in LA at 0.5 ± 0.1, while it was 1.0 ± 0.1 in CK. The expression level of *ndhB* gene reached 5.6 on the 21st day in HA, which was positively correlated with NADPH dehydrogenase activity (45 U/mg protein), while

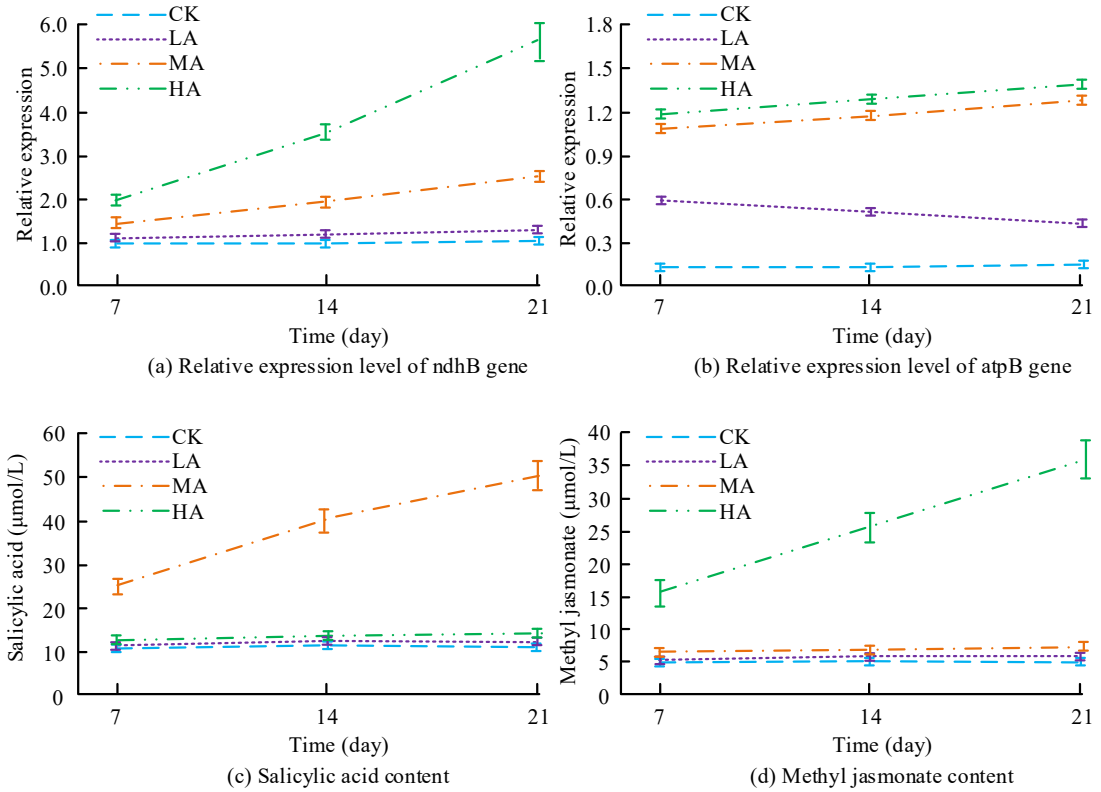

Figure 6. Changes in key gene expression levels and hormone content.

atpB gene was downregulated to 0.4 in the LA group, confirming the effectiveness of RNA interference (Figure 6b). The SA content in MA significantly increased to 50.2 ± 4.0 μmol/L, possibly promoting growth by activating the antioxidant enzyme system, while that in the CK was 10.5 ± 1.0 μmol/L (Figure 6c). The content of methyl jasmonate in HA significantly increased to 35.8 ± 3.0 μmol/L, and synergistic gene overexpression enhanced metabolic EA, compared to 5.2 ± 0.5 μmol/L in CK (Figure 6d). The number of mitochondria and chloroplasts in HA increased, and their structures became more complete. Under high-power microscopy, the numbers of mitochondria per field of view in HA, LA, and CK were 35 ± 3, 15 ± 2, and 20 ± 2, respectively, while the numbers of chloroplasts were 25 ± 2, 10 ± 1, and 15 ± 2, respectively. The number of mitochondria in the MA was 28 ± 3, and the number of chloroplasts was 18 ± 2. Mechanism validation showed that gene overexpression combined with chemical treatment could synergistically enhance activation. The expression level of NADPH dehydrogenase gene in HA was 5.6 times that of CK, and the content of methyl jasmonate reached 35.8 ± 3.0 μmol/L. The number of mitochondria and chloroplasts increased by 75% and 67%, and the structural integrity was significantly optimized.

Acknowledgements

The research was supported by Research Project of Branch Organizations of the Chinese Society for Technical and Vocational Education in 2024 (Grant No. ZJ2024B064), Teacher Research Project of Laiwu Vocational and Technical College in 2023 (Grant No. 2023zdky03), Educational Research Planning Project of Shandong Education Development Promotion Association in 2024 (Grant No. JCHKT2024235).

References

1. Kumar S, Jeevaraj T, Yunus MH, Chakraborty S, Chakraborty N. 2023. The plant cytoskeleton takes center stage in abiotic stress responses and resilience. Plant Cell Environ. 46(1):5-22.
2. Manna M, Rengasamy B, Sinha AK. 2023. Revisiting the role of MAPK signaling pathway in plants and its manipulation for crop improvement. Plant Cell Environ. 46(8):2277-2295.
3. Liang Y, Huang Y, Liu C, Chen K, Li M. 2023. Functions and interaction of plant lipid signaling under abiotic stresses. Plant Biol. 25(3):361-378.
4. Delmer D, Dixon RA, Keegstra K, Mohnen D. 2024. The plant cell wall—dynamic, strong, and adaptable—is a natural shapeshifter. Plant Cell. 36(5):1257-1311.
5. Cosgrove DJ. 2024. Structure and growth of plant cell walls. Nat Rev Mol Cell Biol. 25(5):340-358.
6. Molina A, Jordá L, Torres MÁ, Martín-Dacal M, Berlanga DJ, Fernández-Calvo P, *et al*. 2024. Plant cell wall-mediated disease resistance: Current understanding and future perspectives. Mol Plant. 17(5):699-724.
7. Chieb M, Gachomo EW. 2023. The role of plant growth promoting rhizobacteria in plant drought stress responses. BMC Plant Biol. 23(1):407-429.
8. Talaat NB, Mostafa AA, El-Rahman SNA. 2023. A novel plant growth–promoting agent mitigates salt toxicity in barley (*Hordeum vulgare* L.) by activating photosynthetic, antioxidant defense, and methylglyoxal detoxification machineries. J Soil Sci Plant Nutr. 23(1):308-324.
9. Zhao Q, Guan X, Zhou L, Asad MAU, Xu Y, Pan G, *et al*. 2023. ABA-triggered ROS burst in rice developing anthers is critical for tapetal programmed cell death induction and heat stress-induced pollen abortion. Plant Cell Environ. 46(5):1453-1471.
10. Roychowdhury R, Hada A, Biswas S, Mishra S, Prusty MR, Das SP, *et al*. 2025. Jasmonic acid (JA) in plant immune response: Unravelling complex molecular mechanisms and networking of defense signaling against pathogens. J Plant Growth Regul. 44(1):89-114.
11. Chu HD, Tran YTH, Pham CT, Le TNQ, Tran TTH, Nguyen TQ, *et al*. 2024. Identification of two enzymes for trehalose synthesis and their potential function in growth and development in peanut (*Arachis hypogaea*): Genome analysis of the encoding trehalose synthesis enzymes in peanut. J Trop Life Sci. 14(1):83-94.
12. Truong TDH, Tran TD, Do DT, Trinh TS, Hoang TTH. 2024. Effect of silicon based fertilizer and biochar from crop residues on dry matter accumulation and Si uptake by rice crop in central Vietnam. Indian J Agric Res. 58(4):588-594.
13. Kumar B, Barik AK, Saha B, Patel N, Fatima A. 2024. Influence of crop diversification in potato-based cropping sequence on growth, productivity and economics of potato in red and lateritic soil of West Bengal. Indian J Ecol. 51(1):197-200.
14. Duan S, Al-Huqail AA, Alsudays IM, Younas M, Aslam A, Shahzad AN, *et al*. 2024. Effects of biochar types on seed germination, growth, chlorophyll contents, grain yield, sodium, and potassium uptake by wheat (*Triticum aestivum* L.) under salt stress. BMC Plant Biol. 24(1):487-500.
15. Chi W, Nan Q, Liu Y, Dong D, Qin Y, Li S, *et al*. 2024. Stress resistance enhancing with biochar application and promotion on crop growth. Biochar. 6(1):43-67.
16. Kvitko BH, Collmer A. 2023. Discovery of the Hrp type III secretion system in phytopathogenic bacteria: How investigation of hypersensitive cell death in plants led to a novel protein injector system and a world of inter-organismal molecular interactions within plant cells. Phytopathology. 113(4):626-636.
17. Ali O, Cheddadi I, Landrein B, Long Y. 2023. Revisiting the relationship between turgor pressure and plant cell growth. New Phytol. 238(1):62-69.
18. Ai Y, Wang H, Liu P, Yu H, Sun M, Zhang R, *et al*. 2024. Insights into contrastive cellulose nanofibrils assembly and nanocrystals catalysis from dual regulations of plant cell walls. Sci Bull. 69(24):3815-3819.
19. He B, Wang H, Liu G, Chen A, Calvo A, Cai Q, *et al*. 2023. Fungal small RNAs ride in extracellular vesicles to enter plant cells through clathrin-mediated endocytosis. Nat Commun. 14(1):4383-4397.
20. Argueso CT, Kieber JJ. 2024. Cytokinin: From autoclaved DNA to two-component signaling. Plant Cell. 36(5):1429-1450.
21. Chinthamu N, Karukuri M. 2023. Data science and applications. J Data Sci Intell Syst. 1(1):83-91.